Optimal PML parameters for efficient numerical simulation of waves in an unbounded domain

Y. Liu[1] K. Duru[2] S. Roberts[3]

(Received 31 January 2023; revised 29 October 2023)

Abstract

The perfectly matched layer (PML) is a perfectly non-reflecting layer that simulates the absorption of waves. However, in practice, once the PML is truncated and discretised, the PML is no longer a completely non-reflecting medium. In this article we discuss how to derive optimal PML parameters for the one dimensional acoustic wave equation. Using a multi-block strategy, we present a numerical implementation of the PML that completely eliminates the PML errors. Numerical experiments are presented to verify the analysis.

DOI:10.21914/anziamj.v64.17968, Published 2023-11-07, as part of the Proceedings of the 20th Biennial Computational Techniques and Applications Conference. ISSN 1445-8810. (Print two pages per sheet of paper.)

Contents

1 Introduction

Generally, wave propagation problems occur in large or unbounded domains. However, because of limited computational resources, numerical simulations are always performed in smaller computational domains by introducing artificial boundaries. Thus, in order to ensure the accuracy of numerical simulations, efficient and reliable domain truncation schemes are necessary.

The perfectly matched layer (PML) [4, 1, 2] has emerged as an effective technology to simulate the absorption of waves in numerical wave solvers [10, 13]. The PML is designed to absorb all outgoing waves without reflections, independent of frequencies and angles of incidence. A desirable attribute of the PML is that it can be easily approximated using standard numerical methods [9, 7]. However, in practice, once the PML is truncated and discretised,

the PML is no longer a perfectly absorbing medium. When the PML is used in computation, the primary sources of errors are numerical reflection errors introduced by discrete approximations and the PML modelling error caused by the finite PML width. Numerical reflection errors are mainly caused by the smoothness properties of the PML damping function across the PML interface. The modelling error is the residual outgoing wave which is reflected from the outer PML boundary and travels back through the layer to corrupt the solution. Therefore, the PML parameters must be tuned and optimised in order to enable optimal performance of the PML for practical problems.

For some model problems, such as Maxwell's equations and the acoustic wave equation, there are precise error formulas for the PML modelling error at the continuous level [14, 3, 6]. However, numerical error analysis and optimal PML parameters for discrete PML models have received less attention. There are only a few exceptions, such as Bermudez et al. [5] who used unbounded PML parameters for the Helmholtz equation at the discrete level.

In this study we derive optimal PML parameters for the time-dependent acoustic wave equation in one space dimension. Our main objective is the derivation of effective PML damping parameters, for discrete approximations of a finite width PML. For monomial damping profiles we parameterise the PML damping function such that the PML modeling error is much less than the machine epsilon for IEEE Standard double precision floating-point arithmetic. The PML parameters are optimal, in terms of efficiency, for a piece-wise constant profile. The PML is discretised using the summation-by-parts (SBP) finite difference operators and boundary conditions implemented using the simultaneous approximation term (SAT) [15, 11]. Time integration is performed using the classical fourth order Runge–Kunta method. However, for non-smooth damping functions the standard SBP-SAT method generates large PML reflection errors which pollute the solutions everywhere. Using a multi-block strategy, we derive a stable numerical implementation of the PML that completely eliminates the PML errors. Numerical experiments are presented verifying the analysis.

In Section 2, the PML for the acoustic wave equation is derived. Then perfect matching of PML, PML modeling error and stability of the PML are discussed. In Section 3, we consider numerical approximations and prove numerical stability. Numerical experiments are performed in Section 4, verifying accuracy. In Section 5 we draw conclusions and suggest possible directions for future work. The proofs of the theorems presented in this article are in Appendix A.

2 The PML for the acoustic wave equation

Consider the linear acoustic wave equation in one space dimension:

$$\rho\frac{\partial u(x,t)}{\partial t}+\frac{\partial p(x,t)}{\partial x}=0\,,\quad \frac{1}{\kappa}\frac{\partial p(x,t)}{\partial t}+\frac{\partial u(x,t)}{\partial x}=0\,, \tag{1}$$

where $x\in\Omega\subset\mathbb{R}$ is the spatial variable and $t\geqslant 0$ denotes the time variable. The unknowns are the acoustic pressure p and the particle velocity field u. Here, $\kappa>0$ is the bulk modulus, $\rho>0$ is the density of the medium, we also introduce wave speed $c=\sqrt{\kappa/\rho}$ and acoustic impedance $Z=\rho c$, and define right-going and left-going characteristics, respectively,

$$w_1=\tfrac{1}{2}(Zu+p)\,,\quad w_2=\tfrac{1}{2}(Zu-p)\,. \tag{2}$$

Let us assume that we want to compute the solution of the wave equation on the negative real line, $x\leqslant 0$, and introduce the PML on the positive real line, $x>0$, to absorb outgoing waves. The Laplace transform is defined by

$$\widetilde{u}(x,s)=\int_0^\infty e^{-st}u(x,t)\,dt\,,\quad s=a+ib\,,\quad \Re s=a>0\,. \tag{3}$$

First, take the Laplace transform in time of the wave equation (1), and analytically continue the transformed equation from the real coordinate x to a complex coordinate $\widehat{x}$, to obtain the Laplace space PML equation

$$\rho s\widetilde{u}_\sigma(\widehat{x},s)+\frac{d\widetilde{p}_\sigma(\widehat{x},s)}{d\widehat{x}}=0\,,\quad \frac{1}{\kappa}s\widetilde{p}_\sigma(\widehat{x},s)+\frac{d\widetilde{u}_\sigma(\widehat{x},s)}{d\widehat{x}}=0\,, \tag{4}$$

where $\widetilde{u}_\sigma$ and $\widetilde{p}_\sigma$ denote the velocity and pressure of the PML in the Laplace space. The relationship between x and $\widehat{x}$ is

$$\widehat{x} = x + \frac{1}{s}\int_0^x \sigma(\eta)\,d\eta\,, \quad \frac{d\widehat{x}}{dx} := S_x = 1 + \frac{\sigma}{s}\,, \tag{5}$$

where $\sigma \geqslant 0$ is the damping function, with $\sigma = 0$ if $x \leqslant 0$ and $\sigma > 0$ if $x > 0$. The PML damping function $\sigma > 0$ is a user defined parameter [5, 16, 12] that simulates the absorption of waves in the PML.

Second, using a coordinate transformation, we transform the PML (4) from the complex domain $\widehat{x}$ back to the real domain x. Then we invert the Laplace transform to obtain the PML equation

$$\rho\frac{\partial u}{\partial t} + \frac{\partial p}{\partial x} = -\rho\sigma u\,, \quad \frac{1}{\kappa}\frac{\partial p}{\partial t} + \frac{\partial u}{\partial x} = -\frac{1}{\kappa}\sigma p\,, \quad t \geqslant 0\,. \tag{6}$$

The subscripts are omitted for convenience, that is $p_\sigma \to p$ and $u_\sigma \to u$. When $\sigma = 0$ in (6) we recover the acoustic wave equation (1).

2.1 Perfect matching and PML modelling error

Perhaps, the most important mathematical property of the PML (6) is perfect matching. This means that the restriction of the general solution of PML (6) to the negative real line $x \leqslant 0$ coincides with the general solution of the acoustic wave equation (1). To see this, we note that the general solution of the acoustic wave equation (1) in the Laplace space (for a right-going wave) is

$$\widetilde{u} = u_0 e^{-\frac{s}{c}x} \quad \text{and} \quad \widetilde{p} = p_0 e^{-\frac{s}{c}x}, \quad \Re s = a > 0\,, \tag{7}$$

where $u_0, p_0 \in \mathbb{R}$ and $c > 0$ is the wave speed. Similarly the general solution of the PML (4) is

$$\widetilde{u}_\sigma = u_0 e^{-\frac{s}{c}\widehat{x}} \quad \text{and} \quad \widetilde{p}_\sigma = p_0 e^{-\frac{s}{c}\widehat{x}}\,. \tag{8}$$

By using equation (5) for the complex coordinate $\widehat{x}$ the general solution (8) of the PML in terms of x is

$$\widetilde{u}_\sigma = \widetilde{u} e^{-\Gamma(x)}, \quad \widetilde{p}_\sigma = \widetilde{p} e^{-\Gamma(x)}, \quad \Gamma(x) := \int_0^x \frac{\sigma(\eta)}{c}\, d\eta, \tag{9}$$

where $\Gamma(x)$ is a real, positive continuous and increasing function with $\Gamma(0) = 0$ for any $\sigma(\eta)$. Since $\sigma = 0$ if $x \leqslant 0$ and $\sigma > 0$ if $x > 0$, we have

$$\widetilde{u}_\sigma = \widetilde{u}, \quad \widetilde{p}_\sigma = \widetilde{p}, \quad \forall x \leqslant 0. \tag{10}$$

Thus, the general solution in Laplace space (8) of the PML (6) and the general solution in Laplace space (7) of the acoustic wave equation (1) coincide for all $x \leqslant 0$, and are *perfectly matched* by construction. There are no reflections as waves pass the interface $x = 0$.

For the PML to be exact we must chose $\sigma > 0$ such that $\lim_{x\to\infty} \Gamma(x) = \infty$. From (9) we have $\widetilde{u}_\sigma(\infty) = 0$ and $\widetilde{p}_\sigma(\infty) = 0$. Thus an infinitely wide PML is perfectly non-reflecting and exact. However, in computation the PML must be truncated, resulting in a finite width layer. A finite width PML, although non-reflecting at the interface, will often yield a *modelling error*. Thus, when waves reach the external boundary of the PML at $x = \delta > 0$ and return to the PML interface at $x = 0$, the amplitude of the wave decreases by a factor of $e^{-2\Gamma(\delta)}$ of its original amplitude. For a PML of finite width $\delta > 0$ the relative modeling error is

$$\text{tol} = e^{-2\Gamma(\delta)}. \tag{11}$$

The tolerance $\text{tol} > 0$ is often a user defined input parameter. However, given the layer width $\delta > 0$, we parameterise the PML damping function $\sigma > 0$ such that $\Gamma(\delta)$ is sufficiently large and the modeling error is $\text{tol} = e^{-2\Gamma(\delta)} \sim 0$. The resulting PML model is perfectly non-reflecting at the interface $x = 0$ and nearly-exact.

For a finite PML width $\delta > 0$ we choose a suitable damping function σ such that $\Gamma(\delta)$ is sufficiently large to match the tolerance $\text{tol} > 0$. We consider the

standard monomial damping function

$$\sigma(x) = \begin{cases} 0 & \text{if } x \leqslant 0\,, \\ d_0 (x/\delta)^n & \text{if } x > 0\,, \end{cases} \tag{12}$$

where the constant $d_0 > 0$ is the damping strength and $n \geqslant 0$ controls the smoothness of $\sigma(x)$ at the interface $x = 0$. From (11) and (9) we have

$$\Gamma(\delta) = \frac{d_0}{c} \times \frac{\delta}{n+1}\,, \quad d_0 = c\frac{n+1}{2\delta} \times \ln\left(\frac{1}{\text{tol}}\right). \tag{13}$$

2.2 Stability of the PML

We consider the PML (6) in the computational domain $\Omega = [-L, \delta]$ of length $L + \delta$ with a PML of width $\delta > 0$. Again, when $\sigma = 0$ in (6) we recover the acoustic wave equation (1). We augment (6) with the smooth initial condition

$$u(x,0) = u_0(x)\,, \quad p(x,0) = p_0(x)\,, \tag{14}$$

and the linear boundary conditions

$$\begin{aligned} B_L(u,p) &:= \frac{1-r_L}{2} Zu + \frac{1+r_L}{2} p = 0\,, \quad \text{at } x = -L\,, \quad |r_L| \leqslant 1\,, \\ B_\delta(u,p) &:= \frac{1-r_\delta}{2} Zu - \frac{1+r_\delta}{2} p = 0\,, \quad \text{at } x = \delta\,, \quad |r_\delta| \leqslant 1\,, \end{aligned} \tag{15}$$

where the real parameters r_δ and r_L are boundary reflection coefficients.

Let the energy in the domain be defined by

$$E(t) = \int_\Omega \left(\frac{\rho}{2}u^2 + \frac{1}{2\kappa}p^2\right) dx\,,$$

and introduce the boundary term

$$\text{BT} = u(-L,t)p(-L,t) - u(\delta,t)p(\delta,t)\,. \tag{16}$$

Theorems 1 and 2 below show that the energy $E(t) > 0$ is controlled by the boundary term BT. To be specific the energy $E(t) > 0$ will not grow unboundedly if $BT \leqslant 0$. In particular, for the boundary conditions (15) $r_L = 1$ implies $p = 0$ at $x = -L$, and $r_\delta = 1$ implies $p = 0$ at $x = \delta$, and therefore $BT = 0$ if $r_L = 1$ and $r_\delta = 1$. If $r_L \neq 1$ and $r_\delta \neq 1$ then

$$BT = -\frac{(1+r_L)}{Z(1-r_L)}p^2|_{x=-L} - \frac{(1+r_\delta)}{Z(1-r_\delta)}p^2|_{x=\delta} \leqslant 0.$$

Therefore, the boundary term is never positive.

The following theorem is proven in Appendix A.1.

Theorem 1. *Consider the PML (6) subject to the initial condition (14) and the boundary conditions (15). Then*

$$\frac{dE(t)}{dt} = BT - 2\int_{-L}^{\delta} \sigma\left(\frac{\rho}{2}u^2 + \frac{1}{2\kappa}p^2\right) dx \leqslant 0. \tag{17}$$

To enable the development of a multi-block strategy we consider the domain $\Omega = \Omega_- \cup \Omega_+$, where $\Omega_- = [-L, 0]$ and $\Omega_+ = [0, \delta]$. We solve the wave equation (1) in Ω_- and the PML (6) in Ω_+, and the solutions are then coupled through the perfect matching conditions (10) at the interface $x = 0$. Denote the solutions of u and p in the sub-domains $\Omega_\pm$ with the superscripts $+/-$. The conditions (10) at $x = 0$ are then expressed as $[\![u]\!] := u^+ - u^- = 0$ and $p^- = p^+ = p$. The energy in the sub-domains is

$$E^\pm(t) = \int_{\Omega_\pm} \left(\sigma\frac{\rho}{2}(u^\pm)^2 + \frac{1}{2\kappa}(p^\pm)^2\right) dx.$$

The following theorem is proven in Appendix A.2.

Theorem 2. *Consider the PML (6) subject to the initial condition (14) and the boundary conditions (15) with $|r_\delta|$ and $|r_L| \leqslant 1$. For $E(t) = E^-(t) + E^+(t)$*

we have

$$\frac{dE(t)}{dt} = BT - p[\![u]\!] - 2\int_0^\delta \sigma\left(\frac{\rho}{2}(u^+)^2 + \frac{1}{2\kappa}(p^+)^2\right) dx \leqslant 0\,. \tag{18}$$

Since $[\![u]\!] = 0$, the energy derivative (18) is equivalent to (17).

3 Numerical approximation

We discretise the domain $\Omega = [-L, \delta]$ into N grid points with a uniform spatial step $\Delta x > 0$. Then

$$x_j = -L + (j-1)\Delta x\,, \quad \Delta x = \frac{L+\delta}{N-1}\,, \quad j = 1, 2, \cdots N\,,$$

where $\mathbf{u} = [u_1(t), u_2(t), \cdots u_N(t)]^T$ denotes the semi-discrete scalar field on the grid.

Spatial derivatives on the grid are approximated by diagonal-norm operator $D \in \mathbb{R}^{N\times N}$ [8] such that $(D\mathbf{u})_j \approx \partial u/\partial x|_{x=x_j}$ and

$$D = H^{-1}Q\,, \quad Q + Q^T = \mathrm{diag}(-1, 0, \ldots, 0, 1)\,, \quad H = H^T > 0\,. \tag{19}$$

We consider the diagonal norm SBP operators with $H = \Delta x\,\mathrm{diag}(h_1, h_2, \cdots, h_N)$, where $h_j > 0$ are the weights of a composite quadrature rule. We have

$$(D\mathbf{u})_j = \left.\frac{\partial u}{\partial x}\right|_{x=x_j} + \mathbb{T}_j\,, \tag{20}$$

where the truncation error is

$$\mathbb{T}_j = \begin{cases} \Delta x^\gamma \beta_j \left.\frac{\partial^{\gamma+1} u}{\partial x^{\gamma+1}}\right|_{x_j}\,, & 1 \leqslant j \leqslant s \quad \text{or} \quad (N-s+1) \leqslant j \leqslant N\,, \\ \Delta x^\nu \beta_j \left.\frac{\partial^{\nu+1} u}{\partial x^{\nu+1}}\right|_{x_j}\,, & s < j < (N-s+1)\,. \end{cases} \tag{21}$$

Here, β_j are mesh independent constants, $\gamma \in \{1, 2, \ldots\}$ is the order of accuracy of the D operator close to the boundary, and $\nu \in \{1, 2, \ldots\}$ is the order of accuracy of the D operator in the interior away from the boundary. For traditional SBP operators based on central difference stencils, the interior accuracy is always even, and we have $(\gamma, \nu) = (r, 2r)$, for $r \in \mathbb{N}$. The parameter s indicates the number of grid points close to the boundary where lower (rth) order accurate stencils are used. For the traditional SBP operators used in this study, $r = 1, 2, 3$ and $s = 1, 4, 6$.

A straightforward SBP-SAT approximation of the PML (6) subject to the initial condition (14) and the boundary conditions (15) is

$$\frac{1}{\kappa}\frac{d\mathbf{p}}{dt} + D\mathbf{u} = \mathrm{SAT}_p - \frac{d_x}{\kappa}\mathbf{p}\,, \quad \rho\frac{d\mathbf{u}}{dt} + D\mathbf{p} = \mathrm{SAT}_u - \rho d_x \mathbf{u}\,, \tag{22}$$

where

$$\begin{aligned}
\mathrm{SAT}_p &= \frac{\tau_{11}}{Z} H^{-1} \boldsymbol{e}_1 B_L(u_1, p_1) + \frac{\tau_{12}}{Z} H^{-1} \boldsymbol{e}_N B_\delta(u_N, p_N)\,, \\
\mathrm{SAT}_u &= \tau_{21} H^{-1} \boldsymbol{e}_1 B_L(u_1, p_1) + \tau_{22} H^{-1} \boldsymbol{e}_N B_\delta(u_N, p_N)\,,
\end{aligned}$$

are penalty terms weakly implementing the boundary conditions, and

$$\begin{aligned}
\boldsymbol{e}_1 &= [1, 0, \ldots, 0]^T, \quad \boldsymbol{e}_N = [0, \ldots, 0, 1]^T\,, \\
d_x &= \mathrm{diag}(\sigma(x_1), \sigma(x_2), \cdots, \sigma(x_N))\,.
\end{aligned}$$

The real coefficients τ_{kl} with $k, l = \{1, 2\}$ are penalty parameters to be determined by enforcing stability. Let the discrete energy in the domain be

$$\mathcal{E}(t) = \frac{1}{2\kappa}\mathbf{p}^T H \mathbf{p} + \frac{\rho}{2}\mathbf{u}^T H \mathbf{u} > 0\,,$$

and the numerical boundary term be

$$\mathrm{BT}_{\mathrm{num}} = -(1 - r_L) Z u_1^2 - \frac{(1 + r_L)}{Z} p_1^2 - (1 - r_\delta) Z u_N^2 - \frac{(1 + r_\delta)}{Z} p_N^2 \leqslant 0\,.$$

The following theorem is proven in Appendix A.3.

Theorem 3. *Consider the semi-discrete approximation of the* PML *(22). If* $\tau_{11} = \tau_{21} = \tau_{22} = -1$ *and* $\tau_{12} = 1$, *then*

$$\frac{d\mathcal{E}(t)}{dt} = BT_{num} - 2\left(\frac{1}{2\kappa}\mathbf{p}^T\left(d_x H\right)\mathbf{p} + \frac{\rho}{2}\mathbf{u}^T\left(d_x H\right)\mathbf{u}\right) \leqslant 0\,.$$

Theorem 3 proves the stability of the semi-discrete problem (22). However, the accuracy of (22) is tied to the truncation error $\mathbb{T}$. From (21) the truncation error depends on the smoothness of the solution. If u is the solution of the wave equation, then from (9) the PML solution is $u_\sigma = e^{-\Gamma(x)}u$. If we assume that u is sufficiently smooth, then the smoothness of u_σ depends only on the PML damping function $\sigma(x)$. For example the first and second derivatives of u_σ are

$$\begin{aligned}
\frac{\partial u_\sigma}{\partial x} &= e^{-\Gamma}\left(\frac{\partial u}{\partial x} - \frac{\sigma}{c}u\right),\\
\frac{\partial^2 u_\sigma}{\partial x^2} &= e^{-\Gamma}\left[\frac{\partial}{\partial x}\left(\frac{\partial u}{\partial x} - \frac{\sigma}{c}u\right) - \frac{\sigma}{c}\left(\frac{\partial u}{\partial x} - \frac{\sigma}{c}u\right)\right].
\end{aligned}$$

If the damping σ is discontinuous across the PML interface, then $\partial u_\sigma/\partial x$ is discontinuous and $\partial^2 u_\sigma/\partial x^2$ does not exist. For an rth order accurate SBP-SAT scheme, we require the existence of $(r+1)$th derivatives of the PML solution so that the truncation error $\mathbb{T}_j$ is defined for every point in the domain. Thus the damping function must be sufficiently smooth such that $\sigma \in C^r(\Omega)$. Otherwise, the numerical solution will be polluted by large numerical errors.

A standard SBP-SAT method suffers from large numerical errors when the PML damping is not sufficiently smooth. For non-smooth damping profiles we must avoid differentiating the solution across the discontinuous interface. Here we propose a numerical multi-block procedure to eliminate the numerical error due to lack of smoothness of the PML damping function σ.

We consider the coupled problem $\Omega = \Omega_- \cup \Omega_+$, where $\Omega_- = [-L, 0]$ and $\Omega_+ = [0, \delta]$, with each sub-block $\Omega_\pm$ discretised using a uniform spatial step $\Delta x > 0$, and with boundary conditions (15). At the PML interface $x = 0$

we enforce the interface conditions $p_N^- - p_1^+ = 0$ and $u_N^- - u_1^+ = 0$. These are weakly implemented using penalties

$$\frac{1}{\kappa}\frac{dp^-}{dt} + Du^- = \frac{\tau_1^-}{Z} IT^-, \quad \rho\frac{du^-}{dt} + Dp^- = \tau_1^- IT^-, \tag{23}$$

$$\frac{1}{\kappa}\frac{dp^+}{dt} + Du^+ = \frac{\tau_1^+}{Z} IT^+ - \frac{d_x}{\kappa}p^+, \quad \rho\frac{du^+}{dt} + Dp^+ = \tau_2^+ IT^+ - \rho d_x u^+, \tag{24}$$

where $IT^- = H^{-1}e_N(w_2^- - w_2^+)$ and $IT^+ = H^{-1}e_1(w_1^+ - w_1^-)$, and

$$w_2^- - w_2^+ = \tfrac{1}{2}\left[Z\left(u_N^- - u_1^+\right) - \left(p_N^- - p_1^+\right)\right],$$
$$w_1^+ - w_1^- = \tfrac{1}{2}\left[Z\left(u_1^+ - u_N^-\right) + \left(p_1^+ - p_N^-\right)\right].$$

As before, the real coefficients $\tau_i^\pm$ with $i = \{1, 2\}$ are penalty parameters to be determined by requiring stability. Let the discrete energy in each sub-block be denoted by

$$\mathcal{E}^\pm(t) = \frac{1}{2\kappa}\left(p^\pm\right)^T H\left(p^\pm\right) + \frac{\rho}{2}\left(u^\pm\right)^T H\left(u^\pm\right) > 0,$$

and introduce the numerical interface term

$$IT_{num} = -\frac{1}{Z}(w_2^- - w_2^+)^2 - \frac{1}{Z}(w_1^+ - w_1^-)^2 \leqslant 0.$$

The following theorem is proven in Appendix A.4.

Theorem 4. *Consider the semi-discrete two-block approximation of the* PML (23)–(24)*, and let* $\mathcal{E}(t) = \mathcal{E}^+(t) + \mathcal{E}^-(t) > 0$. *If* $\tau_1^- = 1$ *and* $\tau_1^+ = \tau_2^+ = \tau_2^- = -1$*, then*

$$\frac{d\mathcal{E}}{dt} = IT_{num} - 2\left(\frac{1}{2\kappa}\left(p^+\right)^T\left(d_x H\right)\left(p^+\right) + \frac{\rho}{2}\left(u^+\right)^T\left(d_x H\right)\left(u^+\right)\right) \leqslant 0.$$

Theorem 4 proves the stability of the numerical interface treatment (23)–(24). The accuracy of the numerical solution is independent of the smoothness of the damping function across the PML interface, but depends on the continuity of the solutions which is guaranteed by the perfect matching property (10).

4 Numerical experiments

In this section we perform numerical experiments to verify the anlysis performed in the previous section. We consider a computational domain of length $L = 10$ and a PML of width $\delta = 0.1 \times L$ and parameterise the PML damping function such that modeling error is $\text{tol} = 10^{-50}$. This tol is much less than the machine epsilon for IEEE Standard for double precision floating-point arithmetic.

We consider constant medium parameters $\rho = 1$, $\kappa = 2.2$ and $c = \sqrt{\kappa/\rho}$, with initial conditions

$$u(x, t = 0) = f(x) = 10e^{-1/\omega^2 (x-2.5)^2}, \quad p(x, t = 0) = 0, \quad \omega = 0.3, \quad (25)$$

and boundary conditions (15) with zero reflection coefficients $r_\delta, r_L = 0$ at both boundaries. We discretise the domain with constant spatial step $\Delta x > 0$ and evolve the solution to the final time $t = 7$ using the classical fourth order accurate Runge-Kutta method with time step $\Delta t = \nu_{\text{CFL}} \Delta x / c$, where ν_{CFL} is the Courant–Friedrichs–Levy (CFL) number and we set $\nu_{\text{CFL}} = 1$. We measure the numerical error as the l_2-norm of the difference between the numerical solution and the exact solution

$$u = \frac{1}{2}\left[f(x + ct) + f(x - ct)\right], \quad p = \frac{Z}{2}\left[f(x - ct) - f(x + ct)\right]. \quad (26)$$

We set $\Delta x = 0.02$ and perform numerical experiments using $n = 0, 1, 2$ for the damping function (12). The numerical error at $t = 5.5$ is shown in Figure 1. For the standard SBP-SAT method when damping is discontinuous, $n = 0$ and numerical errors are large, as seen in Figure 1(a). In Figure 1(b), the error decreases for a linear $n = 1$ damping function, but the PML reflection error significantly dominates the error of the numerical method. Setting $n = 2$ improves accuracy, however it increases the magnitude of the damping strength d_0 and this eventually violates the restriction imposed on an explicit time-step by the ν_{CFL}. For $n = 2$, Figure 1(c), shows the solution explodes in the PML and destroys the accuracy of the solution everywhere. For large d_0

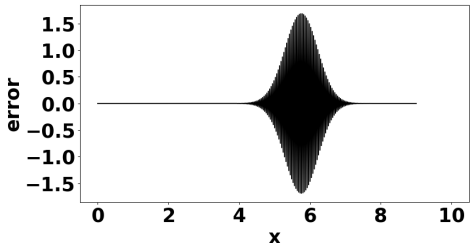

(a) Standard method with $n = 0$

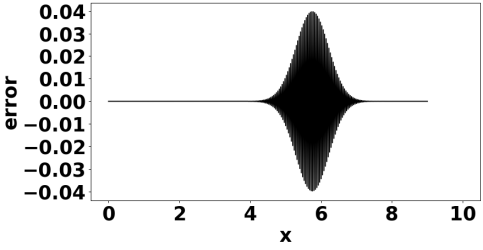

(b) Standard method with $n = 1$

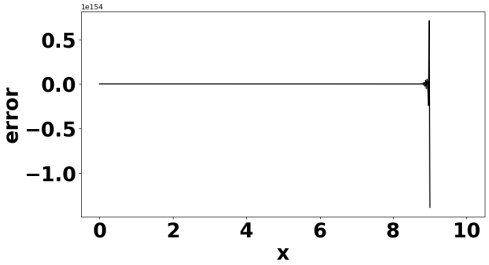

(c) Standard method with $n = 2$

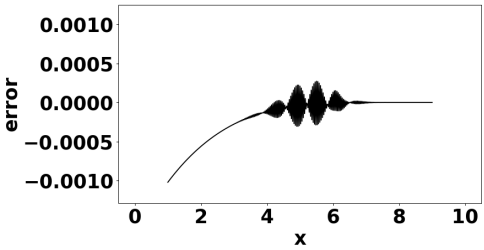

(d) Multi-block method with $n = 0$

Figure 1: Numerical errors for the pressure at time $t = 5.5$ when the damping function σ has degree: (a) $n = 0$; (b) $n = 1$; and (c) $n = 2$, for an SBP operator (SBP6) with sixth order accurate interior stencils; and for (d) $n = 0$ with the multi-block method.

the numerical method is stabilised by reducing the time-step or through an implicit time-stepping method. However, any stabilisation strategy will have a negative impact on the efficiency of the numerical method. For the multi-block SBP-SAT method the numerical error is independent of the smoothness of the damping, as seen in Figure 1(d) with $n = 0$. The multi-block SBP-SAT method avoids differentiating the solution across the discontinuous interface and ensures the accuracy of numerical solutions.

We also perform grid convergence studies. Table 1 is for the standard SBP-SAT method and shows that the non-smoothness of the damping function destroys the convergence properties of the underlying numerical method. Table 2 is

Table 1: The convergence of the error for the standard SBP-SAT method.

Nodes	$n = 0$	Rate	$n = 1$	Rate
201	5.171×10^{-2}	N/A	1.578×10^{-3}	N/A
401	1.725×10^{-2}	1.584	3.339×10^{-4}	2.241
801	7.857×10^{-3}	1.135	8.933×10^{-5}	1.902
1601	3.681×10^{-3}	1.094	2.213×10^{-5}	2.013
3201	1.832×10^{-3}	1.007	5.629×10^{-6}	1.975

Table 2: The convergence of the error for the multi-block SBP-SAT method.

Nodes	$n = 0$	Rate	$n = 1$	Rate
201	4.074×10^{-3}	N/A	4.074×10^{-3}	N/A
401	5.013×10^{-5}	6.345	5.013×10^{-5}	6.345
801	1.086×10^{-6}	5.529	1.086×10^{-6}	5.529
1601	3.182×10^{-8}	5.092	3.182×10^{-8}	5.092
3201	1.015×10^{-9}	4.970	1.015×10^{-9}	4.970

for the multi-block SBP-SAT method, where we preserve the accuracy and the convergence properties of the numerical method, even when the PML damping is discontinuous.

5 Conclusion

We derived and analysed optimal PML parameters for the 1D acoustic wave equation. For monomial profiles we parameterise the PML damping function such that the PML modeling error is much less than the machine epsilon for IEEE Standard double precision floating-point arithmetic. The PML parameters are optimal, in terms of efficiency, for a piece-wise constant profile. We derived provably stable schemes for the PML using the SBP-SAT method. However, for non-smooth damping functions a straightforward SBP-SAT method generates large PML reflection errors which pollute the solutions everywhere. Using a multi-block strategy, we present a numerical implementation of the PML that

completely eliminates the PML errors. Numerical experiments are presented to verify the analysis. The future direction of this research is to extend the 1D result to 2D and 3D problems.

A Appendix

In this appendix we prove the theorems presented in this article.

A.1 Proof of Theorem 1

Proof: We multiply the first equation of (6) by u and multiply the second equation of (6) by p, then integrate with respect to x to obtain

$$\begin{aligned}&\int_{-L}^{\delta}\left(\rho u\frac{\partial u}{\partial t}+\frac{1}{\kappa}p\frac{\partial p}{\partial t}\right)dx+\int_{-L}^{\delta}\left(u\frac{\partial p}{\partial x}+p\frac{\partial u}{\partial x}\right)dx\\&=-\int_{-L}^{\delta}\left(\rho\sigma u^2+\frac{1}{\kappa}\sigma p^2\right)dx\,.\end{aligned}\tag{27}$$

Using integration by parts

$$\begin{aligned}\frac{dE(t)}{dt}&=BT-2\int_{-L}^{\delta}\sigma\left(\frac{\rho}{2}u^2+\frac{1}{2\kappa}p^2\right)dx\,,\\BT&=u(-L,t)p(-L,t)-u(\delta,t)p(\delta,t)\,.\end{aligned}\tag{28}$$

♠

A.2 Proof of Theorem 2

Proof: Introduce the boundary terms

$$BT^{-}=u(-L,t)p(-L,t)-u^{-}p^{-}\,,\quad BT^{+}=u^{+}p^{+}-u(\delta,t)p(\delta,t)\,.$$

From (28) in the proof of Theorem 1 (Appendix A) and PML equation (6), we have

$$\frac{dE^-(t)}{dt} = BT^-, \quad \frac{dE^+(t)}{dt} = BT^+ - 2\int_{-L}^{\delta} \sigma\left(\frac{\rho}{2}u^2 + \frac{1}{2\kappa}p^2\right) dx.$$

Since $p^- = p^+ = p$ we have

$$\frac{d\left[E^-(t) + E^+(t)\right]}{dt} = BT - p[\![u]\!] - 2\int_{0}^{\delta} \sigma\left(\frac{\rho}{2}(u^+)^2 + \frac{1}{2\kappa}(p^+)^2\right) dx.$$

♠

A.3 Proof of Theorem 3

Proof: Let $\tau_{11} = \tau_{22} = \tau_{21} = -1$ and $\tau_{12} = 1$, and multiply the first equation of (22) by $\mathbf{p}^T H$ to obtain

$$\frac{1}{\kappa}\mathbf{p}^T H\frac{d\mathbf{p}}{dt} + \mathbf{p}^T HD\mathbf{u} = -\frac{1-r_L}{2}u_1p_1 - \frac{1+r_L}{2Z}p_1^2 + \frac{1-r_\delta}{2}u_Np_N + \frac{1+r_\delta}{2}p_N^2 - \frac{1}{\kappa}\mathbf{p}^T(d_xH)\mathbf{p}. \quad (29)$$

Then multiply the second equation of (22) by $\mathbf{u}^T H$ to obtain

$$\rho\mathbf{u}^T H\frac{d\mathbf{u}}{dt} + \mathbf{u}^T HD\mathbf{p} = -\frac{1-r_L}{2}Zu_1^2 - \frac{1+r_L}{2}u_1p_1 - \frac{1-r_\delta}{2}Zu_N^2 + \frac{1+r_\delta}{2}u_Np_N - \rho\mathbf{u}^T(d_xH)\mathbf{u}. \quad (30)$$

Sum equations (29) and (30), and use the SBP property (19) to obtain

$$\frac{d\mathcal{E}(t)}{dt} = BT_{num} - 2\left(\frac{1}{\kappa}\mathbf{p}^T(d_xH)\mathbf{p} + \rho\mathbf{u}^T(d_xH)\mathbf{u}\right) \leqslant 0.$$

♠

A.4 Proof of Theorem 4

Proof: Let $\tau_1^- = 1$ and $\tau_1^+ = \tau_2^+ = \tau_2^- = -1$. Multiply the first equation of (23) by $(\mathbf{p}^-)^T\mathbf{H}$ and multiply the second equation of (23) by $(\mathbf{u}^-)^T\mathbf{H}$, then sum them together and use the SBP property (19) to obtain

$$\frac{d\mathcal{E}^-}{dt} = -u_N^- p_N^- + \frac{1}{Z} p_N^-(w_2^- - w_2^+) - u_N^-(w_2^- - w_2^+).$$

Similarly, multiply the first equation of (24) by $(\mathbf{p}^+)^T\mathbf{H}$ and multiply the second equation of (24) by $(\mathbf{u}^+)^T\mathbf{H}$, then sum them together and use the SBP property (19) to obtain

$$\begin{aligned}\frac{d\mathcal{E}^+}{dt} &= u_1^+ p_1^+ - \frac{1}{Z} p_1^+(w_1^+ - w_1^-) - u_1^+(w_1^+ - w_1^-) \\ &\quad - 2\left(\frac{1}{2\kappa}(\mathbf{p}^+)^T(d_x\mathbf{H})(\mathbf{p}^+) + \frac{\rho}{2}(\mathbf{u}^+)^T(d_x\mathbf{H})(\mathbf{u}^+)\right). \end{aligned} \tag{31}$$

We have included interface terms only, and have ignored external boundary terms.

Using (2) we rewrite $\mathbf{u}^-$, $\mathbf{u}^+$, $\mathbf{p}^-$ and $\mathbf{p}^+$ as functions of w_1^-, w_2^-, w_1+ and w_2^+:

$$\begin{aligned}\frac{d\mathcal{E}^-}{dt} &= -\frac{1}{Z}[(w_1^-)^2 + (w_2^-)^2 - 2w_2^- w_2^+], \\ \frac{d\mathcal{E}^+}{dt} &= -\frac{1}{Z}[(w_1^+)^2 + (w_2^+)^2 - 2w_1^- w_1^+] \\ &\quad - 2\left(\frac{1}{2\kappa}(\mathbf{p}^+)^T(d_x\mathbf{H})(\mathbf{p}^+) + \frac{\rho}{2}(\mathbf{u}^+)^T(d_x\mathbf{H})(\mathbf{u}^+)\right).\end{aligned}$$

On summing these two equations together, we obtain

$$\frac{d\mathcal{E}}{dt} = \mathrm{IT}_{\mathrm{num}} - 2\left(\frac{1}{2\kappa}(\mathbf{p}^+)^T(d_x\mathbf{H})(\mathbf{p}^+) + \frac{\rho}{2}(\mathbf{u}^+)^T(d_x\mathbf{H})(\mathbf{u}^+)\right) \leqslant 0.$$

References

[1] D. Appelö, T. Hagstrom, and G. Kreiss. "Perfectly matched layers for hyperbolic systems: General formulation, well-posedness, and stability". In: *SIAM J. Appl. Math.* 67.1 (2006), pp. 1–23. DOI: 10.1137/050639107. (Cit. on p. C79).

[2] D. H. Baffet, M. J. Grote, S. Imperiale, and M. Kachanovska. "Energy decay and stability of a perfectly matched layer for the wave equation". In: *J. Sci. Comput.* 81.3 (2019), pp. 2237–2270. DOI: 10.1007/s10915-019-01089-9 (cit. on p. C79).

[3] E. Bécache and M. Kachanovska. "Stability and convergence analysis of time-domain perfectly matched layers for the wave equation in waveguides". In: *SIAM J. Numer. Anal.* 59.4 (2021), pp. 2004–2039. DOI: 10.1137/20M1330543. (Cit. on p. C80).

[4] J.-P. Berenger. "A perfectly matched layer for the absorption of electromagnetic waves". In: *J. Comput. Phys.* 114.2 (1994), pp. 185–200. DOI: 10.1006/jcph.1994.1159. (Cit. on p. C79).

[5] A. Bermúdez, L. Hervella-Nieto, A. Prieto, and R. Rodríguez. "An optimal perfectly matched layer with unbounded absorbing function for time-harmonic acoustic scattering problems". In: *J. Comput. Phys.* 223.2 (2007), pp. 469–488. DOI: 10.1016/j.jcp.2006.09.018 (cit. on pp. C80, C82).

[6] J. Diaz and P. Joly. "A time domain analysis of PML models in acoustics". In: *Comput. Meth. Appl. Mech. Eng.* 195.29 (2006), pp. 3820–3853. DOI: 10.1016/j.cma.2005.02.031. (Cit. on p. C80).

[7] K. Duru. "The role of numerical boundary procedures in the stability of perfectly matched layers". In: *SIAM J. Sci. Comput.* 38.2 (2016), A1171–A1194. DOI: 10.1137/140976443. (Cit. on p. C79).

[8] K. Duru and E. M. Dunham. "Dynamic earthquake rupture simulations on nonplanar faults embedded in 3D geometrically complex, heterogeneous elastic solids". In: *J. Comput. Phys.* 305 (2016), pp. 185–207. DOI: 10.1016/j.jcp.2015.10.021. (Cit. on p. C86).

[9] K. Duru, A.-A. Gabriel, and G. Kreiss. "On energy stable discontinuous Galerkin spectral element approximations of the perfectly matched layer for the wave equation". In: *Comput. Meth. Appl. Mech. Eng.* 350 (2019), pp. 898–937. DOI: 10.1016/j.cma.2019.02.036. (Cit. on p. C79).

[10] K. Duru and G. Kreiss. "The perfectly matched layer (PML) for hyperbolic wave propagation problems: A review". In: *arXiv*, 2201.03733 (2022). DOI: 10.48550/ARXIV.2201.03733. (Cit. on p. C79).

[11] T. Lundquist and J. Nordström. "The SBP-SAT technique for initial value problems". In: *J. Comput. Phys.* 270 (2014), pp. 86–104. DOI: 10.1016/j.jcp.2014.03.048. (Cit. on p. C80).

[12] R. Martin and C. Couder-Castaneda. "An improved unsplit and convolutional perfectly matched layer absorbing technique for the Navier–Stokes equations using cut-off frequency shift". In: *Comput. Model. Eng. Sci.* 63 (2010), pp. 47–77. DOI: 10.3970/cmes.2010.063.047 (cit. on p. C82).

[13] F. Pled and C. Desceliers. "Review and recent developments on the perfectly matched layer (PML) method for the numerical modeling and simulation of elastic wave propagation in unbounded domains". In: *Arch. Comput. Meth. Eng.* 29 (2021), pp. 471–518. DOI: 10.1007/s11831-021-09581-y. (Cit. on p. C79).

[14] B. Sjögreen and N. A. Petersson. "Perfectly matched layer for Maxwell's equation in second order formulation". In: *J. Comput. Phys.* 209 (2005), pp. 19–46. DOI: 10.1016/j.jcp.2005.03.011 (cit. on p. C80).

[15] M. Svärd and J. Nordström. "Review of summation-by-parts schemes for initial-boundary-value problems". In: *J. Comput. Phys.* 268 (2014), pp. 17–38. DOI: 10.1016/j.jcp.2014.02.031. (Cit. on p. C80).

[16] E. Vitanza, R. Grammauta, D. Molteni, and M. Monteforte. "A shallow water SPH model with PML boundaries". In: *Ocean Eng.* 108 (2015), pp. 315–324. DOI: 10.1016/j.oceaneng.2015.07.054. (Cit. on p. C82).

Author addresses

1. **Y. Liu**, Mathematical Sciences Institute, Australian National University, ACT 2600, AUSTRALIA.
mailto:yijia.liu@anu.edu.au

2. **K. Duru**, Mathematical Sciences Institute, Australian National University, ACT 2600, AUSTRALIA.
mailto:kenneth.duru@anu.edu.au
orcid:0000-0002-5260-7942

3. **S. Roberts**, Mathematical Sciences Institute, Australian National University, ACT 2600, AUSTRALIA.
mailto:stephen.roberts@anu.edu.au
orcid:0000-0002-6730-3108